Nuclear export of ubiquitinated proteins determines the sensitivity of colorectal cancer to proteasome inhibitor

Tingyu Wu[1]*, Wei Chen[1]*, Yongwang Zhong[2]*, Xiaodan Hou[3], Shengyun Fang[2], Chen-Ying Liu[1], Guanghui Wang[1], Tong Yu[1], Yu-Yang Huang[4], Xuesong Ouyang[4], Henry Q.X. Li[4], Long Cui[1#], Yili Yang[3#]

[1]Department of Colorectal Surgery, Xinhua Hospital, Shanghai Jiaotong University School of Medicine, Shanghai, 200095, P. R. China; [2]Center for Biomedical Engineering and Technology, Department of Physiology，University of Maryland School of Medicine, Baltimore, MD21201, U.S. A; [3]Suzhou Institute of Systems Medicine, Center for Systems Medicine Research, Chinese Academy of Medical Sciences, Suzhou, Jiangsu, 215123, P. R. China; [4]Crown Bioscience Inc., 3375 Scott Blvd, Suite 108, Santa Clara, CA 95054, USA

*These authors contributed equally to the study.

[#]Correspondence: Yili Yang, Suzhou Institute of Systems Medicine, Center for Systems Medicine Research, Chinese Academy of Medical Sciences, 218 Xinghu Street, Suzhou, Jiangsu, China, Phone: 86-18702169867, Fax: 86-0512-62873779, E-mail: yyl@ism.cams.cn; Long Cui, Department of Colorectal Surgery, Xinhua Hospital, 1665 Kongjiang Road, Shanghai Jiaotong University School of Medicine, Shanghai, China. Phone: 86-13901745953, Fax: 86-023-25077855, E-mail:

longcuidr@126.com;

Running title: Combination of Bortezomib and KPT330 for colorectal cancer

Key words: proteasome inhibitor; nuclear export inhibition; p53; chemotherapy; colorectal cancer

Financial support: L. Cui are supported by the National Natural Science Foundation of China (Grant No. 81372636). Y. L. Yang are supported by the National Natural Science Foundation of China (Grant No. 81302089).

Disclosure of Potential Conflicts of Interest: No potential conflicts of interest were disclosed.

Other notes: 4128 words, 6 Figures, 1 table

Abstract

Although proteasome inhibitors such as Bortezomib had significant therapeutic effects in multiple myeloma and mantel cell lymphoma, they exhibited minimal clinical activity as a mono-therapy for solid tumors, including colorectal cancer. We found in the present study that proteasome inhibition induced a remarkable nuclear exportation of ubiquitinated proteins. Inhibition of CRM1, the nuclear export carrier protein, hampered protein export and synergistically enhanced the cytotoxic action of Bortezomib on colon cancer cells containing wild type p53, which underwent G2/M cell cycle block and apoptosis. Further analysis indicated that tumor suppressor p53 was one of the proteins exported from nuclei upon proteasome inhibition, and in the presence of CRM1 inhibitor KPT330, nuclear p53 and expression of its target genes were increased markedly. Moreover, knockdown of p53 significantly reduced the synergistic cytotoxic action of Bortezomib and KPT330 on p53+/+ HCT116 cells. In mice, KPT330 markedly augmented the anti-tumor action of Bortezomib against HCT116 xenografts as well as patient-derived xenografts that harbored functional p53. These results indicate that nuclear p53 is a major mediator in the synergistic anti-tumor effect of Bortezomib and KPT330, and provides a rationale for the use of proteasome inhibitor together with nuclear export blocker in the treatment of colorectal cancer. It is conceivable that targeting nuclear exportation may serve as a novel strategy to overcome resistance and raise chemotherapeutic efficacy, especially for the drugs that activate the p53 system.

Introduction

Colorectal cancer (CRC) is one of the most common malignancies with estimated more than 1.2 million new cases each year worldwide. Noteworthily, its incidence rate has been increasing in many developing areas over the last several decades despite the downward trend in developed countries (1). As the majority of patients are diagnosed at advanced stages, and the relapse of the tumor that has become resistance to the 5-fluorouracil- and oxaliplatin-based combination chemotherapy, the 5-year survival rate for patients with CRC remains quite low (2). Thus, early diagnosis through targeted screening and finding new targets and approaches for the treatment are sorely needed to improve the prognosis of individuals with CRC.

It has been shown that alterations of the ubiquitin-proteasome system are critical for cancer initiation and development, often through enhanced degradation of tumor suppressors and reduced degradation of oncoproteins (3, 4). Genomic analyses also revealed that mutations of ubiquitination-related proteins, including APC, p53, Fbw7 and Smad4, are the characteristic changes of CRC (5). Proteasome inhibitors such as Bortezomib are able to induce growth arrest and apoptosis in CRC cells in vitro (6). Bortezomib has also been approved for the treatment of multiple myeloma and mantle cell lymphoma by FDA (7, 8). However, Bortezomib or newer generation of proteasome inhibitors had minimal anti-tumor activity in patients with advanced CRC or other solid tumors (9-11). These results prompted significant efforts to combine proteasome inhibitors with other anti-tumor strategies, including conventional

chemotherapy, radiation and other targeted therapy. At present, the promise of proteasome inhibitors in the treatment of solid tumors has yet to be realized.

Precisely controlled transportation of protein across nuclear membrane is critical for proper growth, death and differentiation of eukaryotic cells (12). It has been shown that chromosome region maintenance 1 (CRM-1) recognizes nuclear export signal (NES) of target proteins and mediates the nuclear export of many tumor suppressor proteins (TSP), such as p53, FOXO, RB1, and CDKN1A (13, 14). CRM-1 is upregulated in a variety of cancers, and responsible for aberrant cytoplasmic localization and inactivation of tumor suppressors. Furthermore, specific CRM-1 inhibitor KPT330 (Selinexor) has broad anti-tumor activity in various tumors and is being actively explored as a novel cancer therapeutic agent (15, 16). FDA has designated Selinexor orphan drug status for certain types of leukemia and lymphoma (17, 18).

In the present study, we examined the nuclear protein exportation upon proteasome inhibitor and KPT330 exposure, proposing possible hypothesis of chemoresistant mechanism of proteasome inhibitors. The synergistic effect and its molecular mechanism of combining Bortezomib and KPT330 on CRC were investigated in vitro and in patient-derived xenografts (PDX) models. The intent of these studies was to provide a rationale for the combination therapy using inhibitors for proteasome and nuclear export in the treatment of CRC.

Materials and Methods

Cell culture

The human cell lines Hela, SW480, SW620, HCT116 and RKO were obtained from American Type Culture Collection (ATCC) in September 2014, which were cultured in Dulbecco's modified Eagle's medium (DMEM; Hyclone, Logan, UT, USA) supplemented with 10% fetal bovine serum (Hyclone, Logan, UT, USA) and 1% penicillin/streptomycin, and were maintained at 37°C in an incubator under an atmosphere containing 5% CO_2. The cell lines were obtained directly from ATCC that performs cell line characterizations or authentication by the short tandem repeat profiling and passaged in our laboratory for fewer than 6 months after receipt.

Cell viability assay

Cell viability assay were determined using the CCK8 method. Briefly, cancer cells were suspended and seeded on 96-well plates (10^3 cells per well) in 100μl culture medium. 24 hours later, the cells were treated with the indicated drugs with another 100μl culture medium for an additional 72h. 10μl of CCK8 reagent (Dojindo, Washington, USA) was added to each well, and the plates were incubated at 37°C for another 2h. The absorbance was measured with a spectrophotometer at 450 nm. Two types of chemotherapeutic drugs, Bortezomib (Selleck, Houston, TX, USA) and KPT330 (Selleck, Houston, TX, USA), were used in our study. The results of the combined treatment were analyzed according to the isobolographic method of Chou and Talalay (19) using the Calcusyn software program. The resulting combination index (CI) was used as a quantitative measure of the degree of interaction between the two drugs. $CI > 1$ indicates additivity, and $CI < 1$ indicates synergism.

Immunofluorescence staining

CRC cells were cultured for 24h prior to drug treatment. Cells were then treated with 5 nM Bortezomib and 100 nM KPT330 for another 24h, then fixed with 4% paraformaldehyde. After blocking with 5% BSA for 1h, slides were incubated overnight with anti-p53 Ab (Santa Cruz Biotechnology, Santa Cruz, CA, USA) and anti-ubiquitinated proteins (Santa Cruz Biotechnology, Santa Cruz, CA, USA). Cells were then washed and incubated with fluorescence conjugated goat anti-rabbit IgG for 1h. Slides were analyzed using Leica Fluorescence Inversion Microscope System.

Western blotting

Western blotting was performed as previously described(20). The following specific antibodies were used for analysis: anti-Cleaved PARP1, anti-Bax, anti-p21, anti-lamin A/C and anti-tublin antibodies were purchased from Cell Signaling Technology Co. (Cell Signaling Technology, Beverley, MA, USA). Anti-actin, anti-p53, anti-ubiquitinated proteins, anti-Mdm2 and anti-Ki67 antibodies were purchased from Santa Cruz Co. (Santa Cruz Biotechnology, Santa Cruz, CA, USA).

Apoptosis assay

For quantification of apoptosis, the Pharmingen^{TM} Annexin V Apoptosis Detection Kit (BD Biosciences, Rockville, MD, USA) was used according to the manufacturer's instructions. Apoptosis was further assessed by the measurement of caspase-3 and -7

activity using a luminometric Caspase-Glo-3/7 assay (Promega, Madison, Wis, USA) according to the manufacturer's protocol.

Flow Cytometric Analysis of Cell Cycle Distribution

Cells were seeded in 6-well plates and allowed to attach overnight. After treated with Bortezomib (5 nM) and KPT330 (100nM) for 48h, cells were fixed with 75% ethanol, stained with RNase-containing PI, and analyzed by flow cytometry after 20 minutes incubation.

Mice xenograft studies

Nude mice (4-6 weeks old, male) were used as an in vivo mouse model. All mouse procedures were approved by the animal care and use committees of Xinhua Hospital. Mice were inoculated subcutaneously in both flanks with HCT116 cells ($2*10^6$), and were randomly divided into four groups. The groups were treated with vehicle (control), Bortezomib (1mg/kg, intraperitoneal administration, b.i.w.), KPT330 (10 mg/kg, oral administration, b.i.w.) or combination of Bortezomib and KPT330. Tumors were measured twice a week with a caliper. Their volumes were calculated as follows: 0.5*length * $width^2$. After 18 days of treatment, the tumors were removed from euthanized mice, photographed, and paraffin imbedded. Tumor Inhibition Rate = (Control Group Volume - Treatment Group Volume) / Control Group Volume × 100%. Tumor inhibition rate >30% was considered as sensitive treatment, tumor inhibition rate <30% was considered as resistant treatment, according to RICIST (Response

Evaluation Criteria in Solid Tumors) criterion (21).

Generation of PDXs from colorectal tumors

Tumor tissue specimens from freshly resected colon were washed and cut into 2- to 3-mm^3 pieces in antibiotic-containing PBS medium. Under anesthesia with pentobarbital, one tumor piece was implanted subcutaneously by a small incision in one side of axilla into 4-6 weeks old male nude mice. Tumors were harvested when they reached a size of 1500 mm^3 (Px1 xenografts). Xenografts from Px1 mice were divided into small pieces and then implanted again subcutaneously as described above to obtain Px2 xenografts. This process was further repeated and the experiments were performed on xenografts Px3.

Immunohistochemistry

Slide sections of tumor specimens were baked at 60 °C for 1h, deparaffinized and rehydrated with xylene and ethanol. After antigen retrieval with microwave heating, endogenous peroxidase activity was blocked with 3% hydrogen peroxide. Non-specific staining was minimized by incubation in 5% FBS. Slides were then incubated with the primary antibodies at 4°C overnight. After washed and incubated with secondary antibodies at room temperature for 1 hour, specific staining was visualized using the Horseradish Peroxidase Color Development Kit (Beyotime, Shanghai, China). Photomicrographs were taken using an Olympus microscope (Center Valley, PA, USA). Expression index = % of positive cells × staining intensity

(1+ 2+ or 3+).

Statistical analysis

Statistical analyses were performed using SPSS 13.0 software. The paired, two-tailed Student's t-test was used to determine the significance between two groups. $P < 0.05$ was regarded as the threshold value for statistical significance.

Results

Proteasome inhibitors promote nuclear protein export

Proteasome inhibition offers an effective strategy to kill tumor cells, and proteasome inhibitors such as Bortezomib have been approved to treat multiple myelomas and lymphoma. However, Bortezomib or newer generation of proteasome inhibitors had minimal anti-tumor activity in patients with advanced CRC or other solid tumors. To explore the potential chemoresistant mechanisms to proteasome inhibitors, we examined the distribution of ubiquitinated proteins in proteasome inhibitor MG132- treated HeLa cells. As revealed by immunofluorescence staining, exposure to MG132 increased ubiquitinated proteins in cells, most notably in cytoplasm, whereas the predominant staining was found in the nuclei in the presence of CRM1 inhibitor LMB (Fig. 1A). Nuclear and cytosolic ubiquitinated proteins were also examined by immunoblotting after the cells were treated with the inhibitors. As shown in Figure 1B, MG132 treatment dramatically increased ubiquitinated proteins in both nuclear and cytoplasmic fractions (Fig. 1B, lanes 5-8 versus 1-4). When

compared with cells treated with MG132 alone, a significantly higher increase of ubiquitinated proteins in the nucleus, as revealed by a higher nuclear/cytoplasmic ratio, was detected in cells simultaneously treated with MG132 and LMB (Fig 1B). We then investigated the distribution of ubiquitinated protein in CRC cells HCT116 and RKO exposed to proteasome inhibitor Bortezomib and CRM1 inhibitor KPT330. Similar to the finding in HeLa cells, ubiquitinated proteins were exported from nuclei upon Bortezomib treatment, and combination of Bortezomib and KPT330 led to increased ubiquitinated protein in the nuclei (Fig. 1C and D). These results indicated that proteasome inhibition promotes the export of ubiquitinated protein from nuclei. It is likely that the nuclear export signals (NESs) in these proteins are responsible for proteasome inhibition-induced nuclear export.

Inhibition of nuclear export enhances the cytotoxic effects of Bortezomib

To assess whether the export of nuclear proteins is related to the cytotoxic action of Bortezomib, colorectal cancer cells HCT116, RKO, SW480 and SW620 cells were cultured in the presence of different concentrations of Bortezomib or KPT330 for 72h. The IC_{50} of different cells indicated that HCT116 and RKO were moderately more resistant to Bortezomib compared with SW480 and SW620 (22 and 99 nM vs. 5 and 9 nM) (Fig. 2A), whereas all of them were relatively insensitive to KPT330 (303, 1790, 1079, and 2345 nM respectively) (Fig. 2A). When CRC cells were treated concurrently with Bortezomib and KPT330 at the indicated concentrations, a markedly greater inhibition of proliferation was observed in all the cells (Fig. 2B and

C, left). Noteworthily, CI (Combination Index) value from isobologram analysis (19) revealed that there is a synergistic effects between Bortezomib and KPT330 in HCT116 (p53 wild type) and RKO (p53 wild type) cells with CI < 1 (Fig. 2B, right), but not in SW480 (p53 mutant) and SW620 (p53 mutant) cells (Fig. 2C, right). Under microscope, there were also profound morphological alterations when the cells were exposed to Bortezomib in the presence of KPT330 (Fig. 2D). To further explore whether the order of drug treatment determines the degree of synergy, HCT116 and RKO cells were treated with Bortezomib and KPT330 at different exposing order. As shown in Supplementary Fig.S1, there were no significant differences in the synergistic action regardless the order. Thus, Bortezomib and KPT330 were given concurrently in the following studies. Furthermore, combination of Bortezomib and KPT330 had significantly increased inhibition on colony formation on HCT116 cells than either drug alone (Fig. 2E). Colony numbers were counted and shown in Fig.2F. These results suggest that the synergistic effects depend on the function of p53. To further confirm that other 20S proteasome inhibitor Carfilzomib exert the similar synergistic effect with KPT330, HCT116 and SW480 cells were treated with Carfilzomib and KPT330 concurrently. Similar to Bortezomib, the cell viability assay and CI values revealed that combinational treatment have synergistic effect on HCT116 rather than SW480 cells (Supplementary Fig. S2 A, B).

To minimize the possibility that the effect of KPT330 is a result of its action on cellular processes other than nuclear exportation, we knocked down CRM1 in HCT116 cells using 2 specific siRNAs. The efficiency of specific siRNA on CRM1

level was confirmed by real-time PCR analysis (Fig. 2G). As shown in Figure 2H, similar to KPT330 treatment, CRM1 knockdown significantly enhanced the cytotoxic effect of Bortezomib. Taken together, these results demonstrated that inhibition of nuclear exportation synergistically enhanced the cell killing activity of proteasome inhibition in p53+/+ colon cancer cells HCT116 and RKO.

Bortezomib and KPT330 induce apoptosis and cell cycle arrest in sensitive cells

To further understand the cytotoxic effects of Bortezomib and KPT330 on HCT116 and RKO cells, annexin V staining and caspase 3/7 activities were assessed using the flow cytometric analysis and luminometric Caspase-Glo-3/7 assay kit. While the relative low doses of each drug alone induced a moderate increase of annexin V staining and caspase 3/7 activation, their combination markedly augmented both the staining and the activation (Fig. 3A and B). The increased annexin V staining was effectively inhibited by the caspase inhibitor Z-VAD-FMK (Fig. 3C). Moreover, The combination of Bortezomib and KPT330 also led to more PARP1 cleavage in HCT116 and RKO cells, indicating synergetic apoptotic effect of the two agents (Fig. 3D). The effects of Bortezomib and KPT330 on cell cycle were further examined. While the compounds alone did not significantly change cell cycles, HCT116 and RKO cells exposed to both Bortezomib and KPT330 underwent a G2/M cell cycle arrest (Fig. 3E), which is a hallmark of p53-mediated cell cycle block (22).

These findings prompted us to examine the action of KPT330 and Bortezomib on tumor xenografts derived from HCT116 cells in nude mice. When the xenografts

became palpable (10-20 mm^3), tumor-bearing nude mice were randomly assigned to receive vehicle, Bortezomib, KPT330 or both (n=10 per group). They showed tolerance to treatment and maintained normal activities. Regular twice a week measurements found no marked changes in body weight. After 18 days of treatment, the mice were euthanized to dissect the tumors. The combination of the drugs significantly enhanced tumor growth inhibition compared with vehicle (83.8% tumor reduction, $p<0.01$), Bortezomib (45.7% tumor reduction, $p<0.01$), or KPT330 (55.2% tumor reduction, $p<0.01$) by the final day of treatment (Fig. 4A). To further confirm the synergistic effect, late stage tumors, with the volume reach ~200 mm^3 before treatment, were also examined (n=6 per group). Similar to the results in Fig. 4A, the combinational treatment group exerted more significant therapeutic action compared with other groups in late stage tumors (Fig. 4B), indicating the synergistic effect of Boretezomib and KPT330 both existed in early and late stage tumors in terms of volume. The expression of p53, Ki67 and DNA fragmentation in the tumors were then evaluated by IHC and Tunel assay (Fig. 4C). Compared with these from vehicle group, Bortezomib treatment decreased the ratio of nuclear/cytoplasmic p53 in the tumor (0.57 vs 0.73, $p<0.01$), whereas KPT330 and Bortezomib combination significantly increased the ratio (2.52 vs 0.73, $p<0.01$) compared with control group (Fig. 4D). Interestingly, the combination of Bortezomib and KPT330 also significantly increased the level of p53 in tumors. Furthermore, compared with vehicle or either drug alone, the combination treatment resulted in significantly reduced level of Ki67 and increased DNA fragmentation, indicating that these tumors had the decreased cell

growth and likely p53-mediated apoptosis (Fig. 4D).

Nuclear p53 plays a critical role in synergistic cytotoxic effect

The level of p53 in cells is mainly controlled through ubiquitination and proteasomal degradation. Association of p53 expression with the cytotoxic effect of KPT330 and Bortezomib prompted us to examine its sub-cellular localization. In CRC cells, accumulated p53 upon Bortezomib treatment was mostly in cytoplasm, whereas co-treatment with KPT330 resulted in a predominant nuclear staining of p53 (Fig. 5A and Supplementary Fig. S3). To further confirm the result, cellular fractionation was performed to examine p53 in nuclei and cytosol by immunoblotting. As shown in Figure 5B and Supplementary Fig. S4A, the results were consistent with the findings from immunofluorescence and indicated that Bortezomib induced nuclear export of p53, whereas it could be effectively blocked by KPT330.

It is conceivable that nuclear retention of p53 might reduce its proteasomal degradation and activate the transcription of its target genes. We therefore analyzed the level of p53 and the expression of its targeted genes p21, Bax, and Mdm2 by western blotting. The results showed that KPT330 further increased Bortezomib-induced p53 accumulation, and the expression of Mdm2, p21, and Bax (Fig. 5C, D and Supplementary Fig. S4B, C). These changes likely account for the synergistic apoptosis and G2/M arrest when HCT116 and RKO cells were treated with Bortezomib and KPT330. To further determine the pivotal role of p53 in the process, we used siRNA to knock down its expression, which was confirmed by real-time PCR

analysis (Fig. 5E and Supplementary Fig. S4D). As shown in Figure 5F and Supplementary Fig. S4E, the synergistic cytotoxic effect of Bortezomib and KPT330 was markedly attenuated by p53 knockdown in HCT116 and RKO cells. It is not clear at this moment whether the lack of complete reverse is due to experimental limitations or involvement of additional factors in the synergistic action. To further confirm whether p53 plays a critical role in the synergistic effect of Carfilzomib, nuclear distribution of p53 was investigated in HCT116 cells exposed to Carfilzomib and KPT330. Similar to the results in Fig. 5A, there was significant nuclear export of p53 upon Carfilzomib exposure, which was inhibited by KPT330 treatment (Supplementary Fig. S2C). When the expression of p53 was knocked down, the synergistic cytotoxicity was largely reversed (Supplementary Fig. S2D).

Patient-derived xenografts contained functional p53 were sensitive to Bortezomib and KPT330 treatment

To further evaluate the potential therapeutic effects of Bortezomib and KPT330, patient-derived primary human CRC xenografts (PDX model) were established and used in our study. We transplanted primary tumor tissues from various CRC patients into nude mice. The clinical pathological features and p53 status were shown in Table 1. After the initial xenografts were established, they were re-implanted into a panel of nude mice to expand the colony (Supplementary Fig. S5A). H&E-stained tumor sections (Model CRC0008) indicated that the initial xenografts and their passages were histologically similar to the original tumors (Supplementary Fig. S5B). We then monitored the growth of 4 PDXs with Bortezomib and KPT330 treatment (Fig.6 A-D,

n=6 per group). Compared with tumors from the control group, Bortezomib or KPT330 alone led to moderately tumor regression by 9.6-36.6 %, whereas their co-treatment inhibited tumor growth more effectively by 60.9-76.7% in CRC0008 (p53 wild type), CRC0014 (p53 wild type) and CRC0005 (p53 wild type) (Fig. 6A, B, C). However, Model CRC0006 (R248G, loss-of-function p53 mutation) was the least responsive to co-treatment with 24% tumor regression (Fig. 6D).

Then tumor sections of Model CRC008 was examined by IHC (Fig. 6E). Similar to the findings in HCT116 xenograft, the ratio of nuclear/cytoplasmic p53 protein was decreased in Bortezomib group compared with the control group (0.49 vs 0.98, $p<0.01$), whereas combination of Bortezomib and KPT330 treatment increased the ratio significantly (2.36 vs 0.98, $p<0.01$) (Fig. 6F). Furthermore, the combination treatment markedly reduced Ki67 expression detected by IHC, and increased apoptosis detected by the Tunel assay (Figure 6F).

To further assess the efficiency of Bortezomib and KPT330 combination treatment, additional primary tumor-derived xenografts from 5 CRC patients were tested (Supplementary Fig. S5C). 3 of the xenografts were sensitive to Bortezomib and KPT330 treatment, and 2 were relatively not sensitive. Among the sensitive xenografts, CRC3496 and CRC3547 contained wild type p53, whereas CRC3405 harbored the C176Y p53 mutation. Interestingly, it has been shown that p53 with C176Y mutation was transcriptional active in a number of experimental systems (23). For the 2 xenografts that are insensitive to the combination treatment, CRC6227 had the loss-of-function p53 mutantion (G245V) (23-25), and CRC3612 contained a wild

type p53. As shown in Table 1, taken together, 6 co-treatment responsive models all possessed functional p53, 2 non-responsive models harbored loss-of-function p53 mutation, whereas only one non-responsive model (CRC3612) harbored wild type p53.

For the purpose of comparison, 5 PDXs (CRC3496, CRC3547, CRC3405, CRC3612, CRC6227) were also treated with various therapeutics, including Cetuximab, Bevacizumab, Cisplatin, Regorafenib, Sorafenib, Doxorubicin, Olaparib, Gefitinib, Everolimus, Everolimus, and Imatinib. The tumor reduction rates of all 13 drugs were produced (Supplementary Fig. S5C). In the 3 PDXs (CRC3496, CRC3547, CRC3405) that are sensitive to Bortezomib and KPT330, co-treatment was the first or second most effective therapeutics compared with other therapeutics. Notably, the two PDX not sensitive to the combination treatment (CRC6227 and CRC3612) were also resistant to cisplatin and doxorubicin, two drugs that act on DNA and are known to induce p53 activation (26, 27). Thus, it is conceivable that the tumor CRC3612 has defect in response to p53. Taken together, these findings provide a rational basis for the clinical use of this combination for the treatment of CRC patients with wild type p53.

Discussion

Despite extensive investigations and clinical trials, development of resistance to chemotherapy remains a major challenge for the treatment of CRC (28). In the effort to explore the mechanisms of the resistance and find novel strategies and targets to

improve the prognosis of CRC patients, we found that proteasome inhibition induced export of ubiquitinated nuclear proteins in CRC cells, which might represent a mechanism of chemoresistance. It has been found that CRM1, the transport protein responsible for nuclear export of many major tumor suppressors and growth regulators, is up-regulated in many tumors (29). Small molecules targeting CRM1 have been developed, and FDA has designated one of the inhibitor Selinexor (KPT330) orphan drug status for certain types of leukemia and lymphoma (17, 18). We demonstrated in this study that inhibition of nuclear export sensitized CRC cells to the cytotoxic action of proteasome inhibitor, which led to G2/M cell cycle block and apoptosis.

Tumor suppressor p53 functions as a critical guardian of genome. In response to genotoxic stimuli, upregulated p53 induced G2/M cell cycle arrest and apoptosis (30, 31). As cellular level of p53 is mainly controlled through ubiquitination-mediated proteasomal degradation, proteasome inhibitors are known to accumulate p53 in cells (32, 33). We found in the study that proteasome inhibition induced nuclear export of p53, and Bortezomib and KPT330 have synergistic cytotoxic action on CRC cell lines with wild type p53 in vitro and in nude mice, but not the cells with mutated p53. In the sensitive cells, the combination treatment led to further increased nuclear p53 and expression of target genes. Furthermore, knockdown of p53 largely abolished the synergistic action. These results indicated that KPT330 and Bortezomib together increases nuclear p53, which in turn initiates the apoptosis program in tumor cells. It is worth noting that both proteasome and CRM1 inhibitors have profound effects on

many cellular processes and may kill tumor cells through a variety of mechanisms. In our study, Bortezomib and KPT330 can effectively kill CRC cells containing mutated p53 (SW480 and SW620). However, their cytotoxic actions are not synergistic in these cells, suggesting the two drugs induced cell death though different pathways in these cells.

While tumor cell line-derived xenografts have been used for decades in assessing cytotoxic action against tumor cells, they are limited in many aspects to mimic human tumors, including reduced intra-tumoral heterogeneity, lack of stromal cells and modest diversity of molecular subtypes (34). Patient-derived xenografts in mice, which largely avoided these limitations and provided a more accurate depictions of human tumors, have become a "gold standard" for evaluating anti-tumor chemotherapeutics (34, 35). It has been shown that the effect of drugs on PDXs from colorectal tumors correlated with clinical outcome (35). We generated primary tumor derived xenografts from 9 patients. The data indicated that the combination of Bortezomib and KPT330 was more effective than either drug alone or other therapeutics in inhibiting tumor growth, and the 6 PDXs that response to the combination therapy all contained functional p53, supporting its further clinical trial. Noteworthily, we also tested a number of therapeutics on these PDXs. The two PDXs that did not response to Bortezomib and KPT330 also failed to be inhibited by the treatment of cisplatin and doxorubicin, 2 drugs that act on DNA and induce p53 (26, 27). It is conceivable that these 2 tumors have defects in p53 signaling pathway.

In summary, our preclinical data suggest that CRC cells could exert self-protective

function upon proteasome inhibition through nuclear export of ubiquitinated proteins, including p53. CRM1 inhibitor KPT330 synergistically sensitizes CRC cells to Bortezomib treatment in vitro and in vivo, through inhibiting nuclear export and restoring functions of p53. Taken together, these findings provide a rational basis for the clinical use of this combination for the treatment of CRC patients with wild type p53.

Acknowledgments:

We acknowledge Jumei Lou for collecting and providing us the patient-derived CRC samples for PDX model establishment.

References

1. Markowitz SD, Bertagnolli MM. Molecular basis of colorectal cancer. New England Journal of Medicine. 2009;361:2449-60.
2. Ebert MP, Tänzer M, Balluff B, Burgermeister E, Kretzschmar AK, Hughes DJ, et al. TFAP2E–DKK4 and chemoresistance in colorectal cancer. New England Journal of Medicine. 2012;366:44-53.
3. Mani A, Gelmann EP. The ubiquitin-proteasome pathway and its role in cancer. Journal of Clinical Oncology. 2005;23:4776-89.
4. Neuss H, Huang X, Hetfeld BKJ, Deva R, Henklein P, Nigam S, et al. The ubiquitin- and proteasome-dependent degradation of COX-2 is regulated by the COP9 signalosome and differentially influenced by coxibs. Journal of Molecular Medicine. 2007;85:961-70.
5. Yang Y, Kitagaki J, Wang H, Hou DX, Perantoni AO. Targeting the ubiquitin‐proteasome system for cancer therapy. Cancer science. 2009;100:24-8.
6. Uddin S, Ahmed M, Bavi P, El-Sayed R, Al-Sanea N, AbdulJabbar A, et al. Bortezomib (Velcade) induces p27Kip1 expression through S-phase kinase protein 2 degradation in colorectal cancer. Cancer research. 2008;68:3379-88.
7. Kane RC, Bross PF, Farrell AT, Pazdur R. Velcade®: US FDA approval for the treatment of multiple myeloma progressing on prior therapy. The oncologist. 2003;8:508-13.
8. Kane RC, Dagher R, Farrell A, Ko C-W, Sridhara R, Justice R, et al. Bortezomib for the treatment of mantle cell lymphoma. Clinical Cancer Research. 2007;13:5291-4.

9. Mackay H, Hedley D, Major P, Townsley C, Mackenzie M, Vincent M, et al. A phase II trial with pharmacodynamic endpoints of the proteasome inhibitor bortezomib in patients with metastatic colorectal cancer. Clinical Cancer Research. 2005;11:5526-33.
10. Kozuch PS, Rocha-Lima CM, Dragovich T, Hochster H, O'Neil BH, Atiq OT, et al. Bortezomib with or without irinotecan in relapsed or refractory colorectal cancer: results from a randomized phase II study. Journal of Clinical Oncology. 2008;26:2320-6.
11. Aghajanian C, Blessing JA, Darcy KM, Reid G, DeGeest K, Rubin SC, et al. A phase II evaluation of bortezomib in the treatment of recurrent platinum-sensitive ovarian or primary peritoneal cancer: a Gynecologic Oncology Group study. Gynecologic oncology. 2009;115:215-20.
12. Kau TR, Silver PA. Nuclear transport as a target for cell growth. Drug discovery today. 2003;8:78-85.
13. Kanai M, Hanashiro K, Kim S-H, Hanai S, Boulares AH, Miwa M, et al. Inhibition of Crm1–p53 interaction and nuclear export of p53 by poly (ADP-ribosyl) ation. Nature cell biology. 2007;9:1175-83.
14. Shao C, Lu C, Chen L, Koty PP, Cobos E, Gao W. p53-Dependent anticancer effects of leptomycin B on lung adenocarcinoma. Cancer chemotherapy and pharmacology. 2011;67:1369-80.
15. Zhong Y, El-Gamal D, Dubovsky JA, Beckwith KA, Harrington BK, Williams KE, et al. Selinexor suppresses downstream effectors of B-cell activation, proliferation and migration in chronic lymphocytic leukemia cells. Leukemia. 2014;28:1158.
16. Tai Y, Landesman Y, Acharya C, Calle Y, Zhong M, Cea M, et al. CRM1 inhibition induces tumor cell cytotoxicity and impairs osteoclastogenesis in multiple myeloma: molecular mechanisms and therapeutic implications. Leukemia. 2014;28:155-65.
17. DiGiulio S. FDA Grants Orphan Drug Status to Selinexor for AML. Oncology Times. 2014.
18. DiGiulio S. FDA's Orphan Drug Status to Selinexor—Now for DLBCL. Oncology Times. 2014.
19. Chou T-C. Drug combination studies and their synergy quantification using the Chou-Talalay method. Cancer research. 2010;70:440-6.
20. Wu T, Wang Z, Liu Y, Mei Z, Wang G, Liang Z, et al. Interleukin 22 protects colorectal cancer cells from chemotherapy by activating the STAT3 pathway and inducing autocrine expression of interleukin 8. Clinical Immunology. 2014;154:116-26.
21. Yoshiaki Tsuchida MD, Patrick Therasse MD. Response evaluation criteria in solid tumors (RECIST): New guidelines. Medical & Pediatric Oncology. 2001;37:1–3.
22. Hock AK, Vousden KH. Tumor suppression by p53: fall of the triumvirate? Cell. 2012;149:1183-5.
23. Shiraishi K, Kato S, Han S-Y, Liu W, Otsuka K, Sakayori M, et al. Isolation of temperature-sensitive p53 mutations from a comprehensive missense mutation library. Journal of Biological Chemistry. 2004;279:348-55.
24. Robert V, Michel P, Flaman JM, Chiron A, Martin C, Charbonnier F, et al. High frequency in esophageal cancers of p53 alterations inactivating the regulation of genes involved in cell cycle and apoptosis. Carcinogenesis. 2000;21:563-5.
25. Crook T, Marston NJ, Sara EA, Vousden KH. Transcriptional activation by p53 correlates with suppression of growth but not transformation. Cell. 1994;79:817-27.
26. Righetti SC, Della Torre G, Pilotti S, Ménard S, Ottone F, Colnaghi MI, et al. A comparative study of p53 gene mutations, protein accumulation, and response to cisplatin-based chemotherapy in advanced ovarian carcinoma. Cancer Research. 1996;56:689-93.
27. Aas T, Børresen A-L, Geisler S, Smith-Sørensen B, Johnsen H, Varhaug JE, et al. Specific P53 mutations are associated with de novo resistance to doxorubicin in breast cancer patients. Nature

medicine. 1996;2:811-4.

28. Dy GK, Hobday TJ, Nelson G, Windschitl HE, O'Connell MJ, Alberts SR, et al. Long-term survivors of metastatic colorectal cancer treated with systemic chemotherapy alone: a North Central Cancer Treatment Group review of 3811 patients, N0144. Clinical colorectal cancer. 2009;8:88-93.

29. Walker CJ, Oaks JJ, Santhanam R, Neviani P, Harb JG, Ferenchak G, et al. Preclinical and clinical efficacy of XPO1/CRM1 inhibition by the karyopherin inhibitor KPT-330 in Ph+ leukemias. Blood. 2013;122:3034-44.

30. Kuerbitz SJ, Plunkett BS, Walsh WV, Kastan MB. Wild-type p53 is a cell cycle checkpoint determinant following irradiation. Proceedings of the National Academy of Sciences. 1992;89:7491-5.

31. Speidel D. Transcription-independent p53 apoptosis: an alternative route to death. Trends in cell biology. 2010;20:14-24.

32. Mitsiades N, Mitsiades CS, Richardson PG, Poulaki V, Tai Y-T, Chauhan D, et al. The proteasome inhibitor PS-341 potentiates sensitivity of multiple myeloma cells to conventional chemotherapeutic agents: therapeutic applications. Blood. 2003;101:2377-80.

33. Maki CG, Huibregtse JM, Howley PM. In vivo ubiquitination and proteasome-mediated degradation of p53. Cancer Research. 1996;56:2649-54.

34. Kopetz S, Lemos R, Powis G. The promise of patient-derived xenografts: the best laid plans of mice and men. Clinical Cancer Research. 2012;18:5160-2.

35. Fichtner I, Slisow W, Gill J, Becker M, Elbe B, Hillebrand T, et al. Anticancer drug response and expression of molecular markers in early-passage xenotransplanted colon carcinomas. European journal of cancer. 2004;40:298-307.

Number	Gender	Age	Tumor	Type	TNM Staging	Differentiation	p53 mutation	p53 function	Bortezomib+ KPT330
CRC0008	male	73	rectum	adenocarcinoma	Ⅲ	Ⅱ	wild type	normal	sensitive
CRC0005	female	61	rectum	adenocarcinoma	Ⅱ	Ⅱ	wild type	normal	sensitive
CRC0014	male	71	rectum	adenocarcinoma	Ⅲ	Ⅲ	wild type	normal	sensitive
CRC0006	female	82	colon	mucinous adenocarcinoma	Ⅲ	Ⅲ	R248G	loss of function	resistant
CRC3496	male	65	colon	adenocarcinoma	Ⅳ	Ⅱ-Ⅲ	wild type	normal	sensitive
CRC3547	male	72	rectum	mucinous adenocarcinoma	Ⅳ	Ⅲ	wild type	normal	sensitive
CRC3405	female	57	colon	adenocarcinoma	Ⅳ	Ⅱ-Ⅲ	C176Y	normal	sensitive
CRC6227	female	61	rectum	adenocarcinoma	Ⅲ	Ⅱ-Ⅲ	G245V	loss of function	resistant
CRC3612	female	68	rectum	adenocarcinoma	Ⅳ	Ⅱ-Ⅲ	wild type	normal	resistant

Table 1. Clinical pathological features and p53 status of PDXs.

Figure legends

Figure 1.

Nuclear transportation of ubiquitinated proteins upon proteasome and nuclear export inhibitor treatment. (A) HeLa cells were treated with MG132 (30 μM) and Leptomycin B (LMB, 20 nM) for 12h as indicated. The cells were fixed and stained for ubiquitin-conjugated proteins (FK2). The nucleus was stained with DAPI. (B) HeLa cells were treated with MG132 (30 μM) and LMB (20 nM) for 12h as indicated followed by fractionation into nuclear (N) and cytoplasmic (C) fractions. Equal amount of proteins from these fractions were processed for immunoblotting with an anti-ubiquitin antibody. Tubulin and Histone H3 were detected as markers for cytoplasmic and nuclear fractions, respectively. Band densities of lanes 5-8 in polyUb blotting were measured. The relative N/C ratios were calculated from 3 independent experiments ($p<0.01$, **). (C, D) HCT116 and RKO cells were treated with Bortezomib (5nM) and KPT330 (100nM) for 12h as indicated. The cells were fixed and stained for ubiquitin-conjugated proteins (FK2). Bars represent 10 μm.

Figure 2.

Bortezomib and KPT330 exhibit synergistic cytotoxicity in HCT116 and RKO cells. (A) SW480, SW620, HCT116 and RKO cells were cultured in 96-well plates and incubated with the different doses of Bortezomib or KPT330 for 72h. Effects on proliferation were assayed by CCK8 experiment. IC_{50} of both drugs were calculated. (B, C) Colorectal cancer cells were treated concurrently with Bortezomib and KPT330 at the indicated concentrations for 72h. Cell viability was measured by CCK8. The synergistic cytotoxicity was quantitatively analyzed by Combination Index (CI) using the Calcusyn software program. Each dots represented one combinational treatment group. CI > 1 indicates additivity, and CI < 1 indicates synergism. (D) Cellular morphology alteration in response to drug treatment for 72h was observed with inverted microscope. (E) Clone formation assay of HCT116 with treatment of Bortezomib or KPT330 alone or combination. (F) Colony formation numbers were counted from 3 independent experiments ($p<0.01$, **). (G) The knockdown efficiency of siRNA of CRM1 was confirmed by real-time PCR analysis. (H) After knocking down the expression of CRM1, HCT116 cells were treated with or without Bortezomib (5nM) for 72h. CCK8 assay was performed to detect cell viability in different groups. The bars represent the mean ± SEM of triplicates in one experiment. ($p<0.01$, **).

Figure 3.

Bortezomib and KPT330 enhance apoptosis in HCT116 and RKO cells. (A) HCT116

and RKO cells were treated with Bortezomib, KPT330 or their combination for 48h at the indicated concentrations. The cells were subsequently stained with annexin V, apoptotic cells were distinguished by flow cytometric analysis. (B) Measurement of caspase-3 and -7 by means of a luminometric assay was performed in cells receiving the same treatment. (C) HCT116 was treated for 48h with 5nM Bortezomib in combination with 100nM KPT330 in the presence of 4 μM pancaspase inhibitor Z-VAD-FMK, stained with annexin V, and analyzed by flow cytometry. (D) The 48h treatment with the combination of Bortezomib and KPT330 increased expression of cleaved PARP1. (E) HCT116 and RKO cells were treated with Bortezomib (5nM), KPT330 (100nM) or their combination for 48 h. Cells were fixed and stained with PI followed by flow cytometric analysis for DNA content. The bars represent the mean ± SEM of triplicates in one experiment. ($p<0.01$, **).

Figure 4.

Bortezomib and KPT330 co-treatment inhibit HCT116 xenografts in nude mice. (A) Relative tumor growth of early stage HCT116 xenografts (10-20 mm^3) treated with vehicle (control), 1 mg kg/ml of Bortezomib, 10 mg/kg of KPT330 or in combination measured from 0 to 18 days post treatment. (n=10 per group). (B) Relative tumor growth of late stage HCT116 xenografts (200 mm^3) receiving the same treatment conditions. (n=6 per group). (C) Immunohistochemical staining of p53, Ki67 and DNA fragmentation in tumor tissues. (D) Quantitative statistics of the Immunohistochemical staining. Bars represent 100 μm. The data shown represent the

mean ± SEM. ($p<0.01$, **).

Figure 5.

Nuclear p53 plays a critical role in synergistic cytotoxic effect. (A) Immunofluorescence with p53 antibody in HCT116 and RKO after treatment with Bortezomib (5nM) or KPT330 (100nM) for 12 h. Bars represent 10 μm. (B) HCT116 cells were treated with Bortezomib (5nM) or KPT330 (100nM) for 12h. Nuclear (N) and cytoplasmic (C) Extracts were separated and subjected to western blotting using p53 antibody. (C) HCT116 cells were treated with Bortezomib (5nM) or KPT330 (100nM) for 12h and subjected to western blotting using various antibodies as indicated. (D) Band densities of results in Fig. 5C were measured. (E) The knockdown efficiency of siRNA of p53 was confirmed by real-time PCR analysis. (F) After knocking downing the expression of p53, HCT116 cells were treated with Bortezomib (5nM) or KPT330 (100nM) for 72h. Scrambled siRNA served as negative control. CCK8 assay was performed to detect cell viability in different groups. The bars represent the mean ± SEM of triplicates in one experiment. ($p<0.01$, **).

Figure 6.

Bortezomib and KPT330 co-treatment inhibit patients-derived xenografts in nude mice. (A-D) Relative tumor growth of PDX models treated with vehicle (control), 1mg kg/ml of Bortezomib, 10mg/kg of KPT330 or in combination measured from 0 to 21 days (n=6 per group). (E, F) Representative H&E and IHC stained sections of

CRC0008 and corresponding quantitative analysis. Bars represent 100 μm. The data shown represent the mean ± SEM. ($p<0.05$,*; $p<0.01$, **).

Fig.1

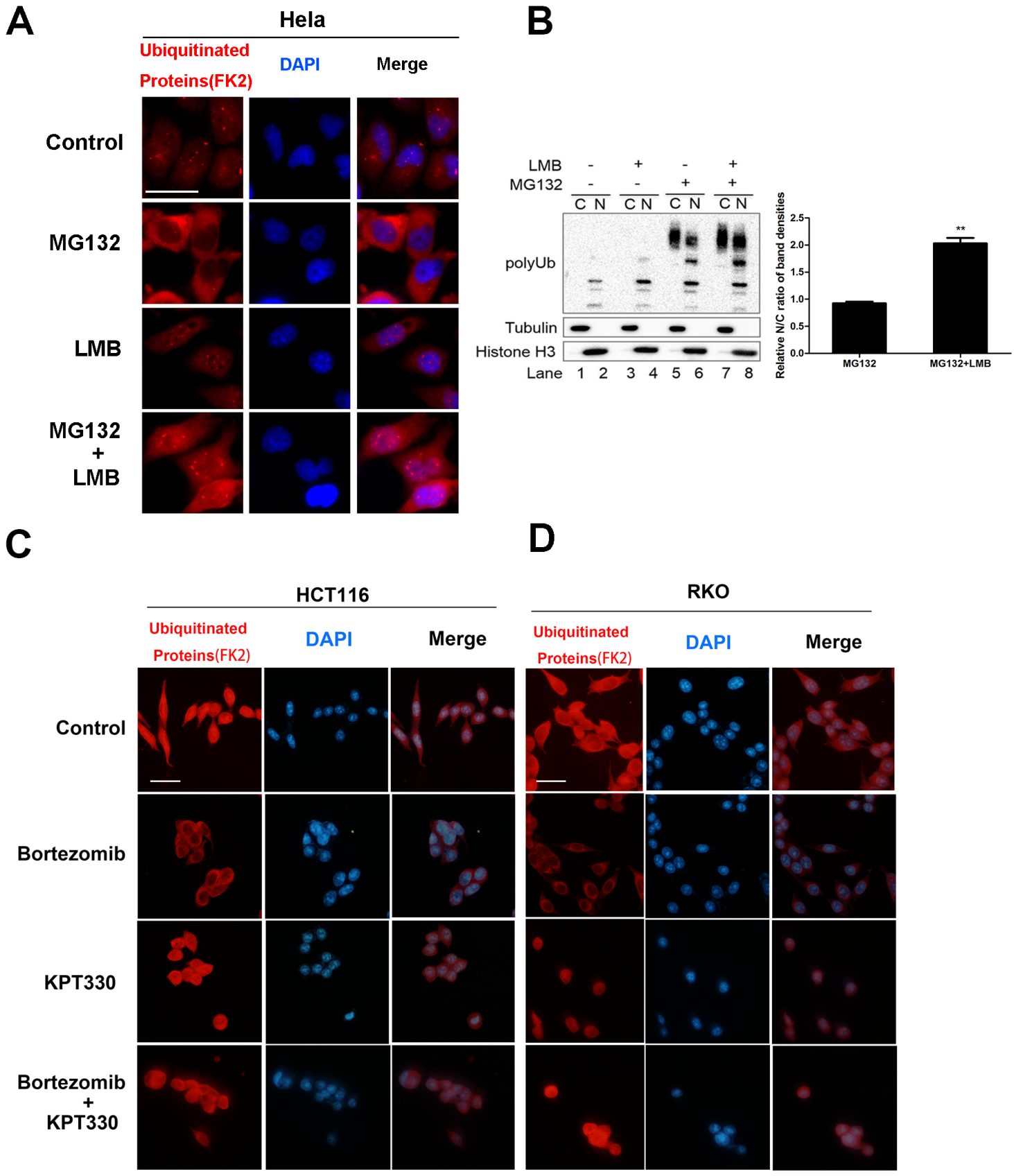
A
Hela
Ubiquitinated Proteins(FK2)
DAPI
Merge
Control
MG132
LMB
MG132 + LMB
B
LMB
MG132
C N C N C N C N
polyUb
Tubulin
Histone H3
Lane 1 2 3 4 5 6 7 8
Relative N/C ratio of band densities
2.5
2.0
1.5
1.0
0.5
0.0
**
MG132
MG132+LMB
C
HCT116
Ubiquitinated Proteins(FK2)
DAPI
Merge
Control
Bortezomib
KPT330
Bortezomib + KPT330
D
RKO
Ubiquitinated Proteins(FK2)
DAPI
Merge

Fig. 2

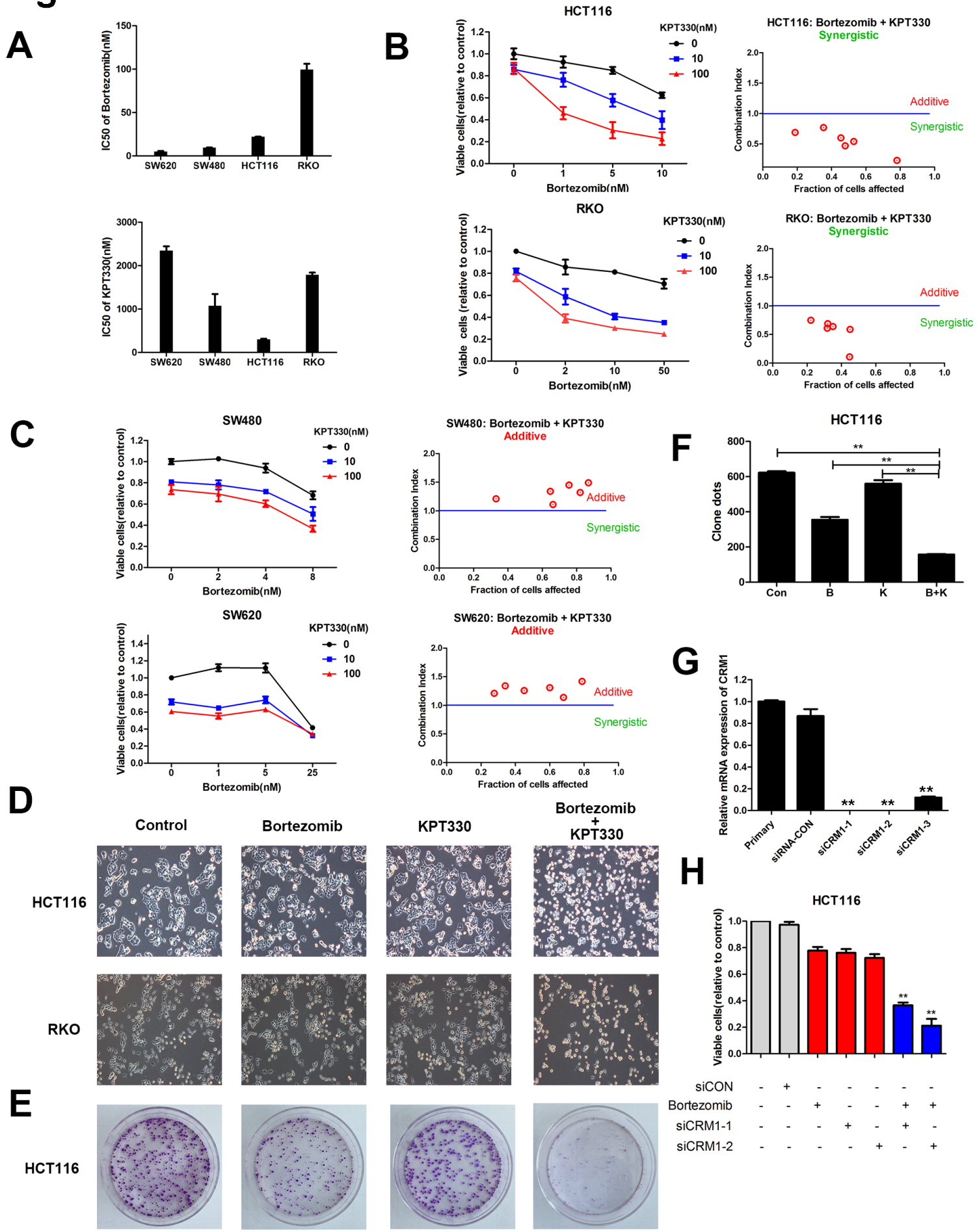
A
IC50 of Bortezomib(nM)
SW620
SW480
HCT116
RKO
IC50 of KPT330(nM)
B
HCT116
KPT330(nM)
0
10
100
Viable cells(relative to control)
Bortezomib(nM)
HCT116: Bortezomib + KPT330
Synergistic
Additive
Combination Index
Fraction of cells affected
RKO
RKO: Bortezomib + KPT330
C
SW480
SW480: Bortezomib + KPT330
Additive
SW620
SW620: Bortezomib + KPT330
F
HCT116
Clone dots
Con
B
K
B+K
G
Relative mRNA expression of CRM1
Primary
siRNA-CON
siCRM1-1
siCRM1-2
siCRM1-3
D
Control
Bortezomib
KPT330
Bortezomib + KPT330
HCT116
RKO
H
HCT116
Viable cells(relative to control)
siCON
Bortezomib
siCRM1-1
siCRM1-2
E
HCT116

Fig. 3

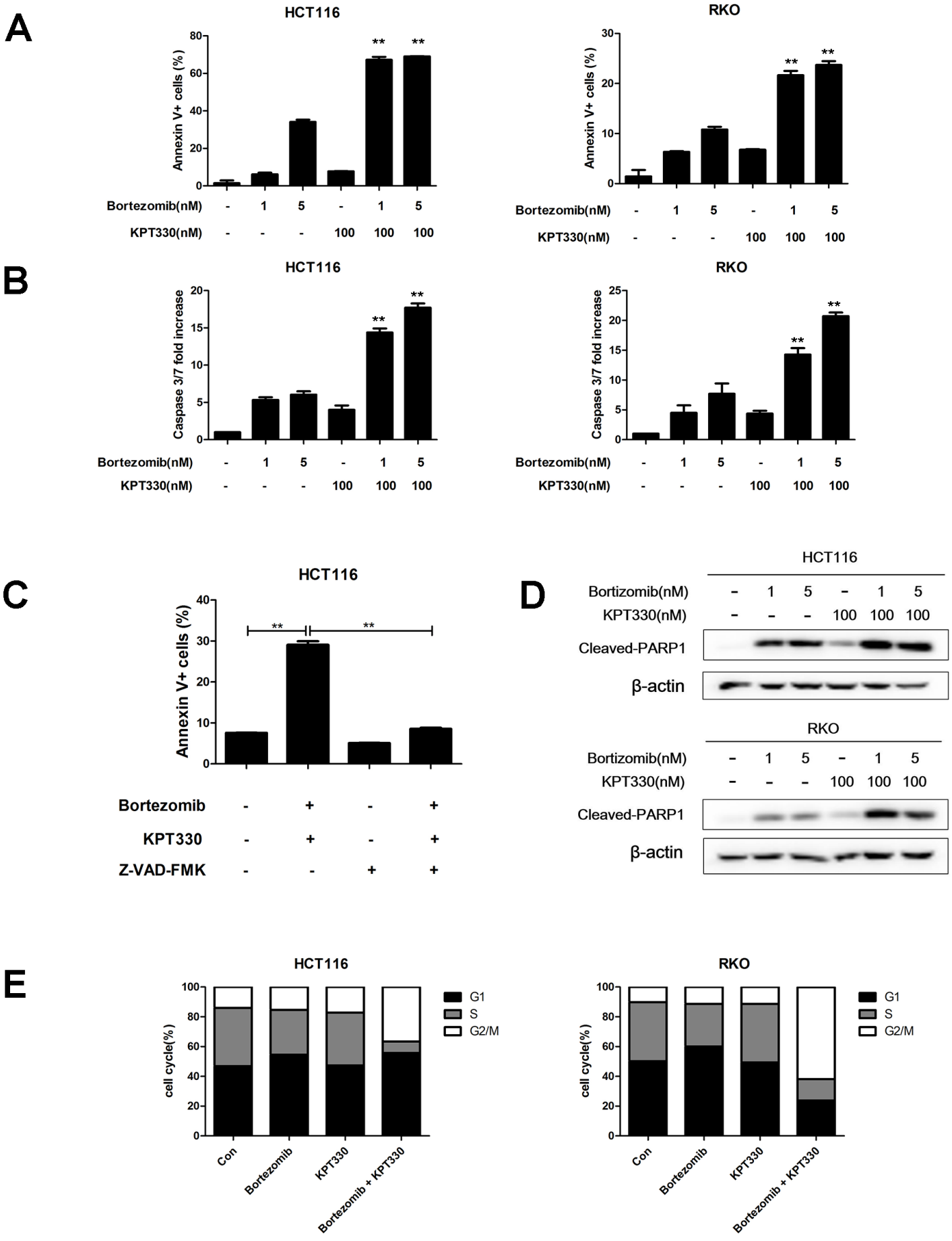
A
HCT116
Annexin V+ cells (%)
Bortezomib(nM) - 1 5 - 1 5
KPT330(nM) - - - 100 100 100
RKO
Annexin V+ cells (%)
Bortezomib(nM) - 1 5 - 1 5
KPT330(nM) - - - 100 100 100
B
HCT116
Caspase 3/7 fold increase
Bortezomib(nM) - 1 5 - 1 5
KPT330(nM) - - - 100 100 100
RKO
Caspase 3/7 fold increase
Bortezomib(nM) - 1 5 - 1 5
KPT330(nM) - - - 100 100 100
C
HCT116
Annexin V+ cells (%)
Bortezomib - + - +
KPT330 - + - +
Z-VAD-FMK - - + +
D
HCT116
Bortizomib(nM) - 1 5 - 1 5
KPT330(nM) - - - 100 100 100
Cleaved-PARP1
β-actin
RKO
Bortizomib(nM) - 1 5 - 1 5
KPT330(nM) - - - 100 100 100
Cleaved-PARP1
β-actin
E
HCT116
cell cycle(%)
G1
S
G2/M
Con
Bortezomib
KPT330
Bortezomib + KPT330
RKO
cell cycle(%)
G1
S
G2/M
Con
Bortezomib
KPT330
Bortezomib + KPT330

Fig. 4

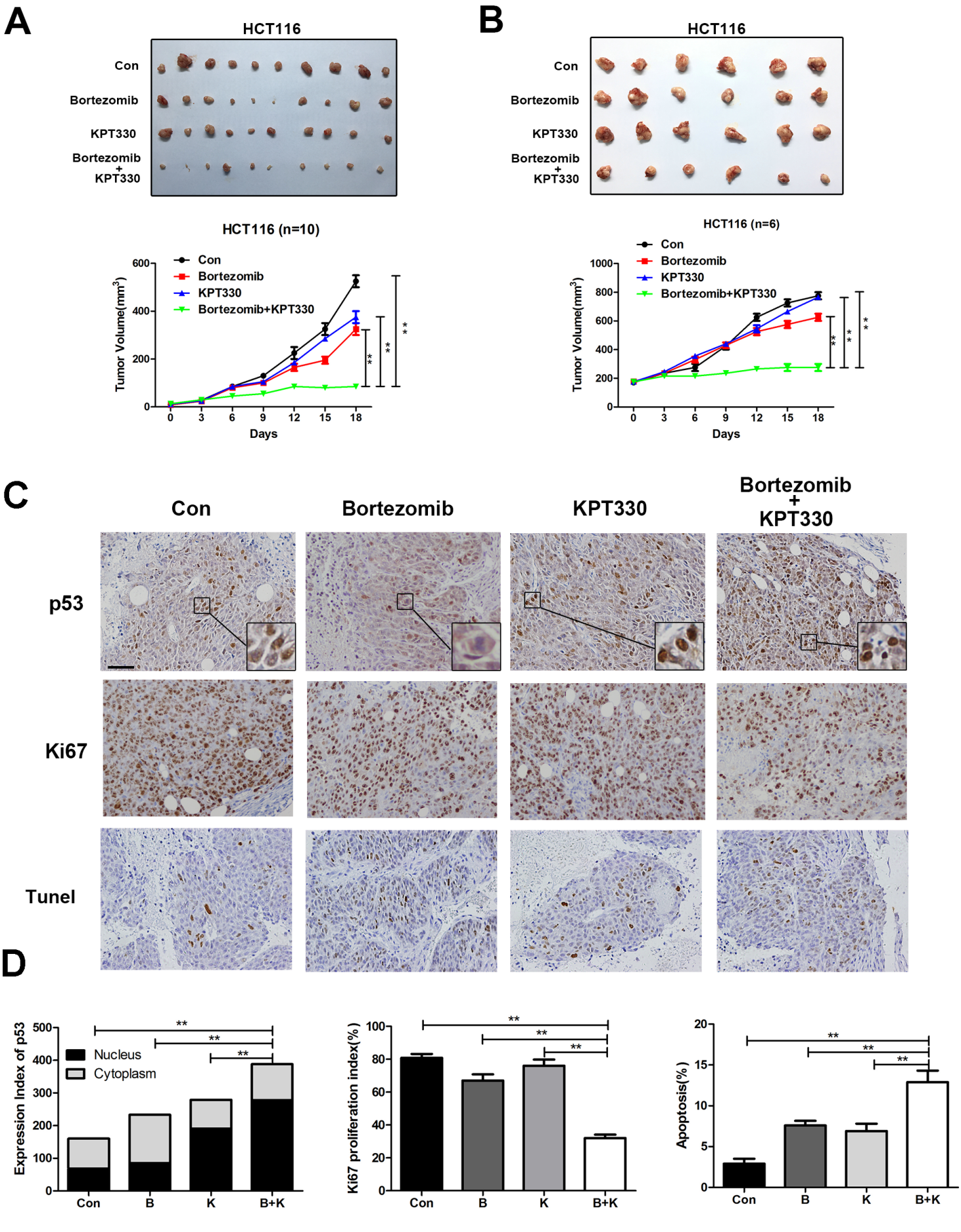
A
HCT116
Con
Bortezomib
KPT330
Bortezomib + KPT330
HCT116 (n=10)
Con
Bortezomib
KPT330
Bortezomib+KPT330
Tumor Volume(mm3)
Days
B
HCT116
Con
Bortezomib
KPT330
Bortezomib + KPT330
HCT116 (n=6)
Con
Bortezomib
KPT330
Bortezomib+KPT330
Tumor Volume(mm3)
Days
C
Con
Bortezomib
KPT330
Bortezomib + KPT330
p53
Ki67
Tunel
D
Expression Index of p53
Nucleus
Cytoplasm
Con
B
K
B+K
Ki67 proliferation index(%)
Apoptosis(%)

Fig. 5

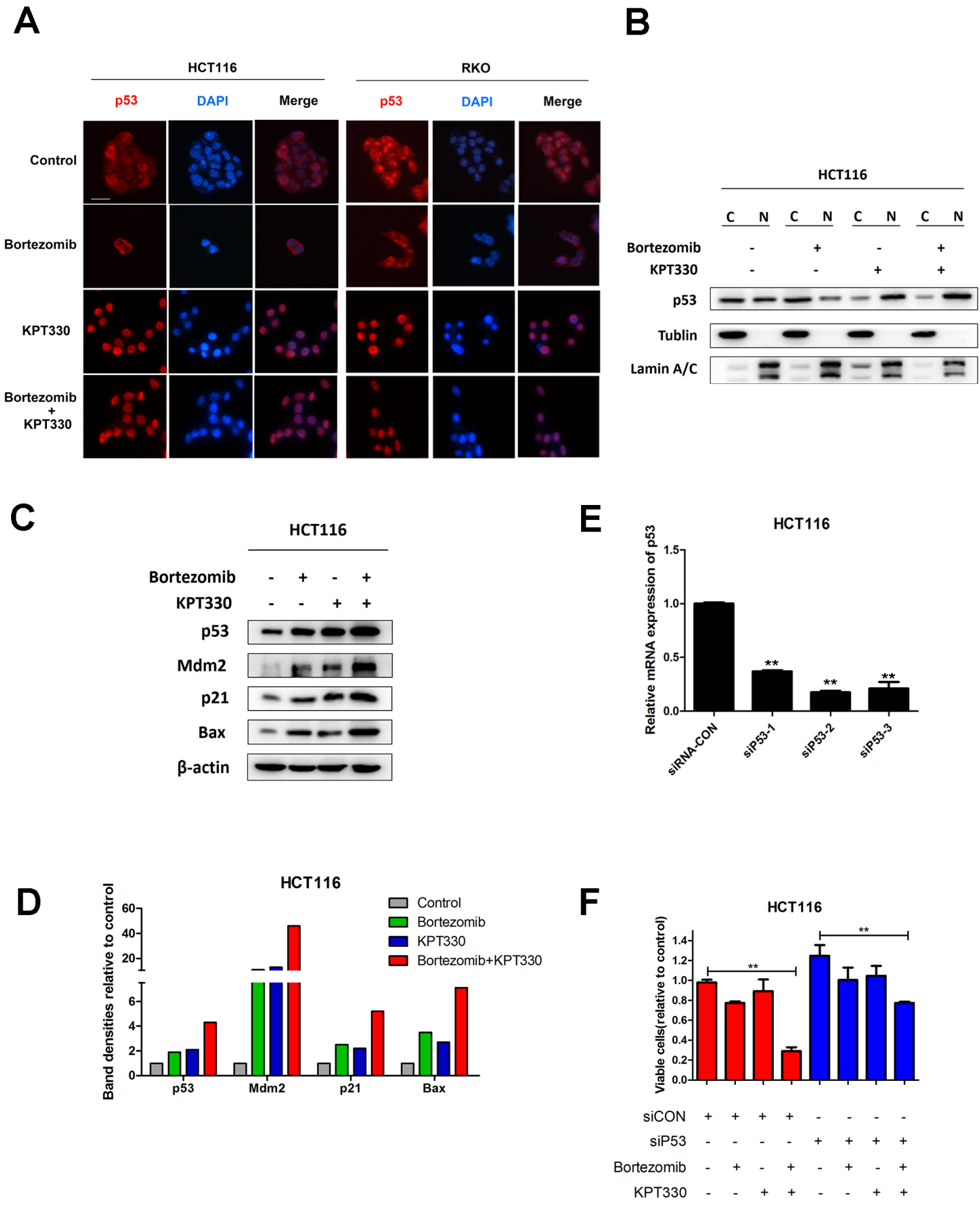
A
HCT116
RKO
p53
DAPI
Merge
Control
Bortezomib
KPT330
Bortezomib + KPT330
B
HCT116
C N C N C N C N
Bortezomib - + - +
KPT330 - - + +
p53
Tublin
Lamin A/C
C
HCT116
Bortezomib - + - +
KPT330 - - + +
p53
Mdm2
p21
Bax
β-actin
D
HCT116
Band densities relative to control
Control
Bortezomib
KPT330
Bortezomib+KPT330
p53
Mdm2
p21
Bax
E
HCT116
Relative mRNA expression of p53
siRNA-CON
siP53-1
siP53-2
siP53-3
F
HCT116
Viable cells(relative to control)
siCON + + + + - - - -
siP53 - - - - + + + +
Bortezomib - + - + - + - +
KPT330 - - + + - - + +

Fig. 6

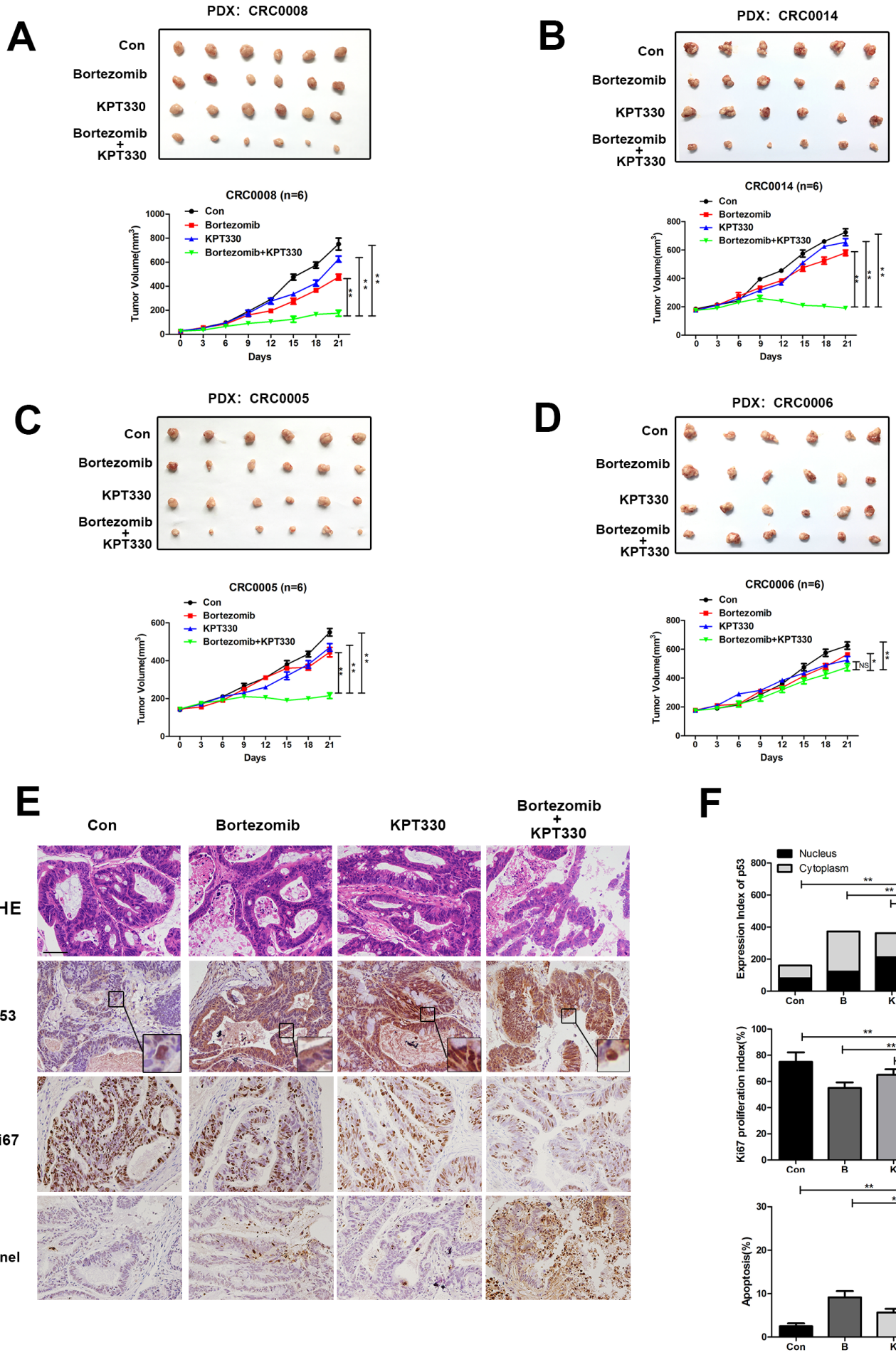
A
PDX: CRC0008
Con
Bortezomib
KPT330
Bortezomib + KPT330
CRC0008 (n=6)
Con
Bortezomib
KPT330
Bortezomib+KPT330
Tumor Volume(mm3)
Days
B
PDX: CRC0014
Con
Bortezomib
KPT330
Bortezomib + KPT330
CRC0014 (n=6)
Con
Bortezomib
KPT330
Bortezomib+KPT330
Tumor Volume(mm3)
Days
C
PDX: CRC0005
Con
Bortezomib
KPT330
Bortezomib + KPT330
CRC0005 (n=6)
Con
Bortezomib
KPT330
Bortezomib+KPT330
Tumor Volume(mm3)
Days
D
PDX: CRC0006
Con
Bortezomib
KPT330
Bortezomib + KPT330
CRC0006 (n=6)
Con
Bortezomib
KPT330
Bortezomib+KPT330
Tumor Volume(mm3)
Days
E
Con
Bortezomib
KPT330
Bortezomib + KPT330
HE
p53
Ki67
Tunel
F
Nucleus
Cytoplasm
Expression Index of p53
Con
B
K
B+K
Ki67 proliferation index(%)
Apoptosis(%)